Chemical Engineering Journal 398 (2020) 125639

Contents lists available at ScienceDirect

Chemical Engineering Journal

journal homepage: www.elsevier.com/locate/cej

Expanded linear polarization response and excellent energy-storage properties in $(Bi_{0.5}Na_{0.5})TiO_3$-$KNbO_3$ relaxor antiferroelectrics with medium permittivity

Jinhai Huang[1], He Qi[1], Ya Gao, Aiwen Xie, Yuhan Zhang, Yifan Li, Siyue Wang, Ruzhong Zuo*

Institute of Electro Ceramics & Devices, School of Materials Science and Engineering, Hefei University of Technology, Hefei 230009, PR China

HIGHLIGHTS

- Excellent comprehensive energy-storage performances of W_{rec} of ~5.2 J/cm^3 and large η of ~88%.
- Relaxor AFE with medium permittivity and expanded linear polarization response.
- Outstanding temperature and frequency stability of W_{rec} in 0.84BNT-0.16KN.
- Enhanced dielectric breakdown strength induced by sub-micron grains.

GRAPHICAL ABSTRACT

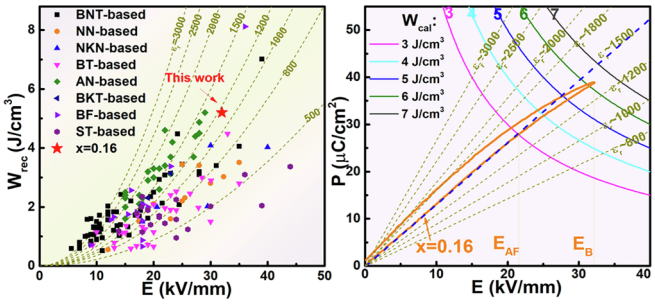

ARTICLE INFO

Keywords:
Energy storage capacitor
Relaxor antiferroelectrics
$(B_{i0.5}Na_{0.5})TiO_3$
Lead-free

ABSTRACT

Dielectric materials with both high recoverable energy-storage density W_{rec} and efficiency η have attracted a lot of attention in recent years. Permittivity plays a crucial role in simultaneously achieving high polarization strength and large applied electric fields for any kinds of dielectric materials, among which antiferroelectric ceramics exhibit giant potentials in energy storage. Adjustment of permittivity has seemed to be more in linear dielectrics, but much less cared about in polar dielectrics so far for high-power energy-storage applications. In this work, a novel lead-free solid solution of $(1\text{-}x)(Bi_{0.5}Na_{0.5})TiO_3$-$xKNbO_3$ was reported to show excellent comprehensive energy-storage performances of W_{rec} of ~5.2 J/cm^3, large η of ~88%, fast discharge rate of $t_{0.9} < 200$ ns and outstanding temperature and frequency stability at $x = 0.16$. The X-ray, Raman spectra and scanning electron microscopy and so on demonstrate that it was basically ascribed to the formation of relaxor antiferroelectric phases with temperature-stable dielectric response and expanded linear polarization response, as well as enhanced dielectric breakdown strength induced by sub-micron grains. Particularly, selection of an appropriately medium permittivity value of about one thousand enables the studied AFE composition bring its superiority into full play in energy-storage properties, as demonstrated by a comparison between W_{rec} values of most previously-reported lead-free ceramics and theoretically predicted ones for linear dielectrics. These findings achieved in current work would provide an important guidance for compositionally designing high-performance energy-storage dielectrics in terms of modifying dielectric properties and polarization responses, particularly for relaxor antiferroelectrics with linear-like characteristics.

* Corresponding author.
E-mail address: piezolab@hfut.edu.cn (R. Zuo).
[1] Contribute equally.

https://doi.org/10.1016/j.cej.2020.125639
Received 7 April 2020; Received in revised form 21 May 2020; Accepted 24 May 2020
Available online 27 May 2020

1. Introduction

Among the majority of electrical storage technologies, dielectric capacitors are suitable for high-power/pulse-power systems owing to their high charge/discharge rates [1–4]. The recoverable energy-storage density (W_{rec}) and efficiency (η) of a capacitor can be determined according to the polarization-electric field (P-E) loop during a charge-discharge period using the following formula: $W_{rec} = \int_{P_r}^{P_{max}} EdP$, $W_{loss} = \int PdE$, and $\eta = W_{rec}/(W_{rec} + W_{loss})$, where P_{max} is the saturated polarization, P_r is the remanent polarization, and W_{loss} is the area of hysteresis loop [5,6]. As a result, energy-storage properties should be determined by ΔP ($=P_{max} - P_r$), breakdown strength E_B, and particularly the shape of P-E loops. P_r is usually a result of irreversible domain switching for ferroelectrics (FEs) or the hysteresis of phase transition as well as domain back-switching for antiferroelectrics (AFEs). However, it can be easily reduced down to nearly zero by introducing dielectric relaxation behavior [3,4,7–9], leading to the improvement of ΔP. Even though E_B is in the range of 20–40 kV/mm for most of bulk ceramics, it can be still effectively enhanced by optimizing the preparation process [10–25], such as hot-pressed technique, spark plasma sintering and tape-casting method. As a result, the optimization of ΔP and E_B values has been most frequently used to enhance the W_{rec} value.

Actually, energy-storage properties for a polar dielectric can be also affected by the characteristics of polarization versus electric field response, i.e., the shape of P-E loops. The rapid increase of polarization caused by domain switching or phase transition under a relatively low

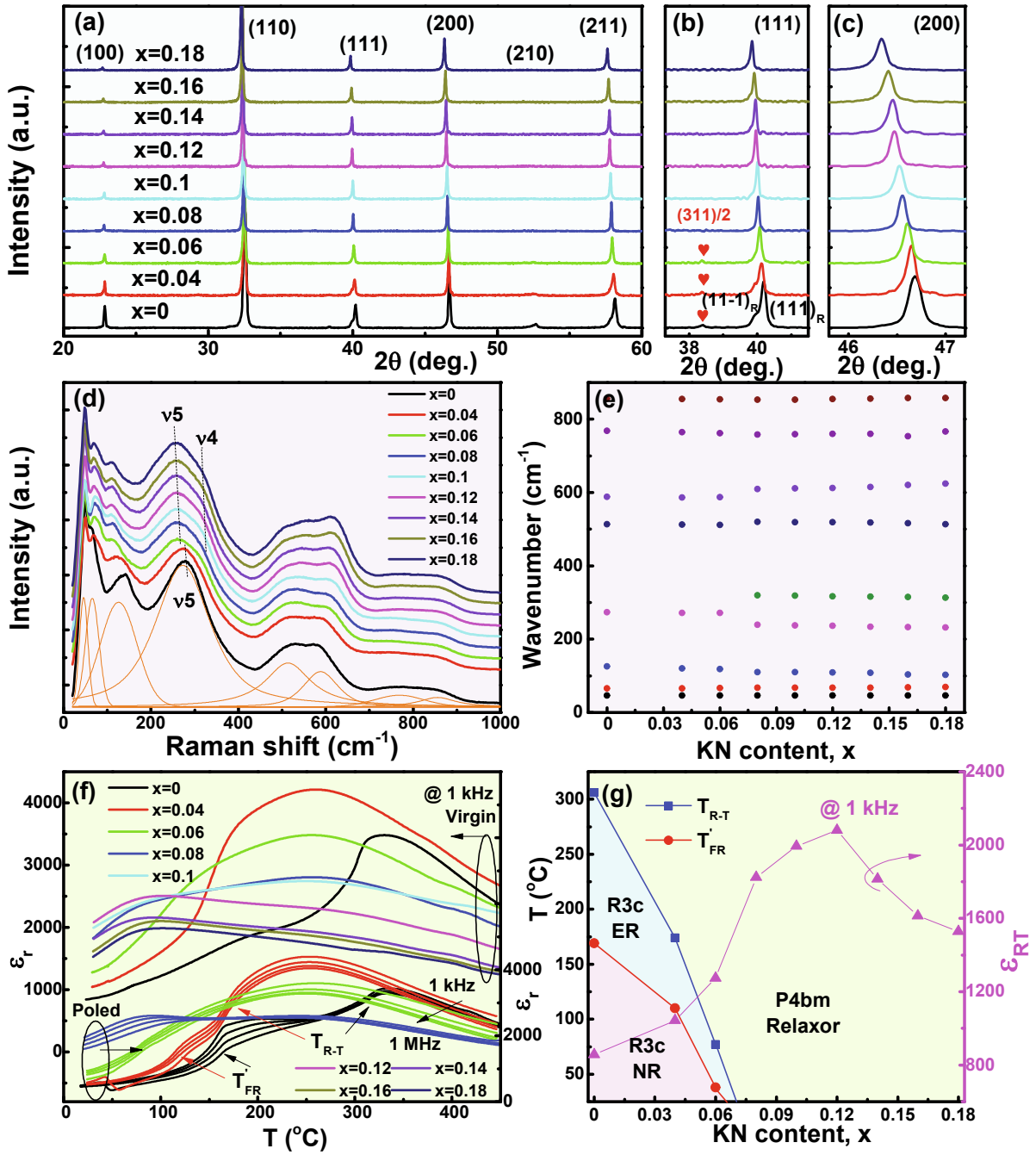

Fig. 1. (a) XRD patterns and locally magnified diffraction peaks around (b) 39° and (c) 47° for (1-x)BNT-xKN ceramics; (d) Raman spectra and (e) the composition dependent wavenumber of Raman modes for (1-x)BNT-xKN samples; (f) temperature and frequency dependent dielectric permittivity (ε_r) of virgin and poled (1-x) BNT-xKN samples; (g) phase diagram of (1-x)BNT-xKN system together with the evolution of room-temperature dielectric permittivity ε_{RT} with KN content.

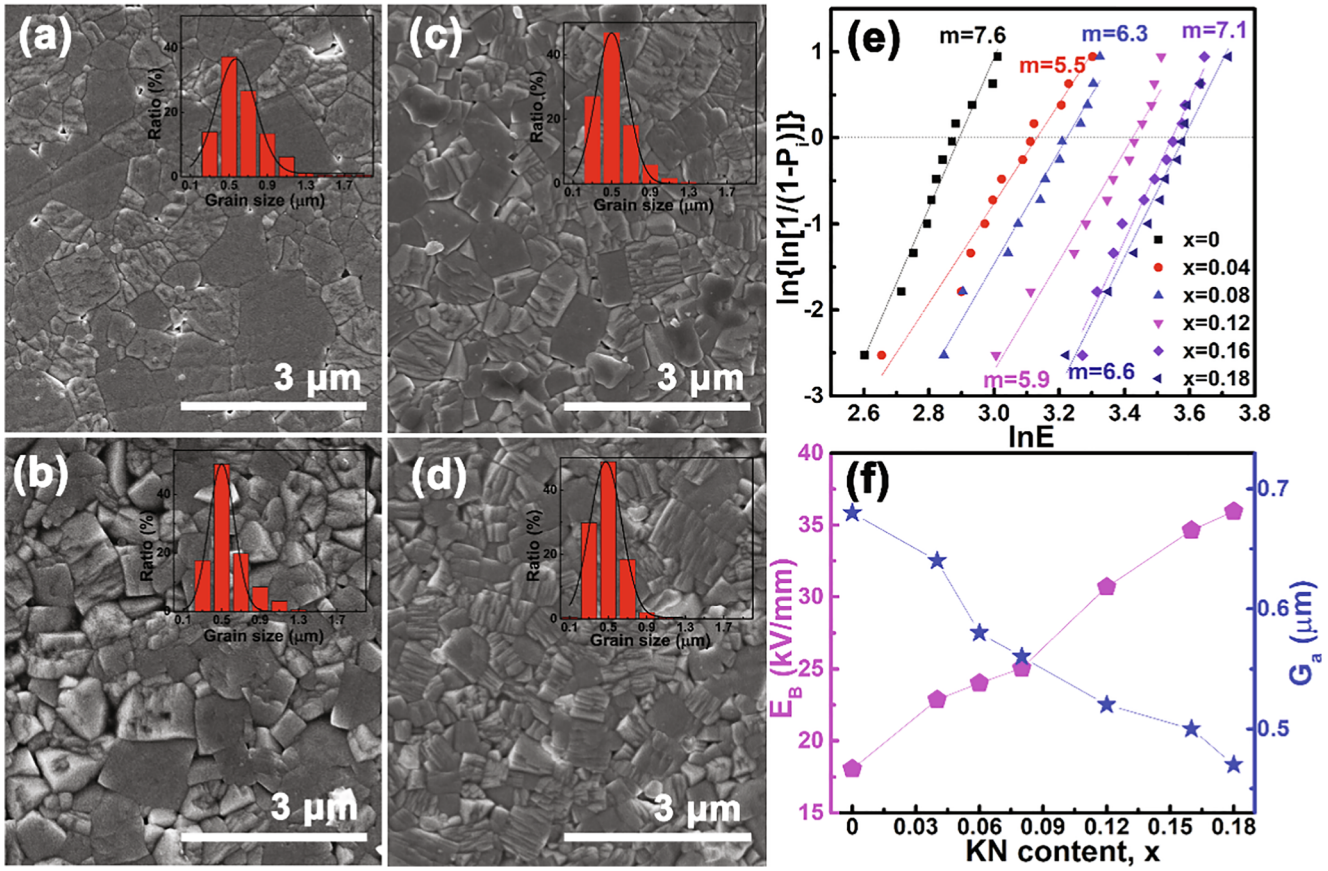

Fig. 2. SEM micrographs and statistical analysis of grain size distribution for (1-*x*)BNT-*x*KN ceramics sintered at their optimum temperatures: (a) $x = 0$, (b) $x = 0.06$, (c) $x = 0.12$ and (d) $x = 0.18$; (e) *Weibull* distributions and fitting lines of the E_B value, and (f) the calculated E_B and average grain size G_a as a function of KN content.

electric field [26] would greatly limit further improvement of W_{rec} value through largely increasing electric field magnitudes. Delaying the polarization saturation under electric fields was thought to be a promising way of increasing energy density [5]. AFE ceramics have large potentials in dielectric energy-storage capacitors owing to reversible AFE-FE phase transition [6,20–25]. However, the adjustment of linear polarization response is critical, which corresponds to the part where the applied field is less than the driving field of AFE to FE phase transition (E_{AF}). Larger line slope (i.e., higher permittivity because $\varepsilon = dP/dE$) and higher E_{AF} values prove to be advantageous for AFE energy-storage capacitors. In addition, the optimization of the nonlinear polarization response under an electric field higher than E_{AF} was also frequently used for enhancing energy-storage properties [3,6,13,20–25]. This is because serious polarization hysteresis, large volume change, and large polarization current would make normal AFEs exhibit low energy-storage efficiency and bad fatigue behavior. Introducing relaxor features in AFEs has proved to be an effective way to delay the polarization saturation process through adjusting the growth and further switching process of antipolar nanoregions (APNRs) [3,14,25–29]. Moreover, the fast response of APNRs to external fields enables an ideal η, in addition to enhanced dielectric response.

$((Bi_{0.5}Na_{0.5})TiO_3$ (BNT)-based ceramics have large potential for generating ultrahigh energy storage properties and outstanding charge-discharge performances [7,13–18], exhibiting obvious advantages for energy storage capacitors owing to their special structures. On the one hand, large spontaneous polarization over 40 μC/cm^2 can be detected in BNT owing to the A-site "lone pair" effect [30]. On the other hand, owing to the compositional disorder on A-site and antiparallel off-centering displacement between A and B-site cations, relaxor and AFE features can be achieved simultaneously in BNT (at high temperature) [31]. In this work, a tetragonal perovskite $KNbO_3$ (KN) was added to stabilize the high-temperature tetragonal AFE phase in BNT close to room temperature [32,33], and simultaneously introduce the dielectric relaxation behavior and achieve adjustable temperature-stable dielectric response. Excellent comprehensive energy storage properties can be obtained in the 0.84BNT-0.16KN ceramic with medium dielectric permittivity.

2. Experimental procedures

Ceramics with compositions of (1-*x*)BNT-*x*KN ($x = 0 \sim 0.18$) were synthesized by a conventional solid-state reaction method using commercially available reagent-grade oxides and carbonate powders as the starting materials. The (1-x)BNT-xKN powders were weighed and mixed thoroughly in ethanol using zirconia balls for 6 h according to their compositional formula. The power was calcined at 850 °C for 2 h. The calcined powders were ball-milled again for 12 h together with 1 mol% SiO_2 as sintering aids, and then pressed into disk samples with a diameter of 10 mm under 100 MPa using polyvinyl alcohol (PVA) as a binder. Sintering was performed in the temperature range of 1050 ~ 1100 °C for 2 h in covered alumina crucibles after burning out the binder at 550 °C for 4 h. Silver electrodes were painted and then fired on both sides of the samples at 550 °C for 30 min.

The room temperature crystal structure was analyzed by a powder X-ray diffractometer (XRD, D/MAX-RB, Rigaku, Tokyo, Japan) using a Cu Kα radiation (λ = 1.5406 Å). Raman spectra were collected on well-polished pellets by 532 nm excitation using a Raman spectrometer (LabRam HR Evolution, HORIBA JOBIN YVON, Longjumeau Cedex, France). Dielectric properties as a function of temperature and frequency were measured by an LCR meter (Agilent E4980A, Santa Clara, CA). The grain morphology was observed by using a field-emission scanning electron microscope (FE-SEM, SU8020, JEOL, Tokyo, Japan).

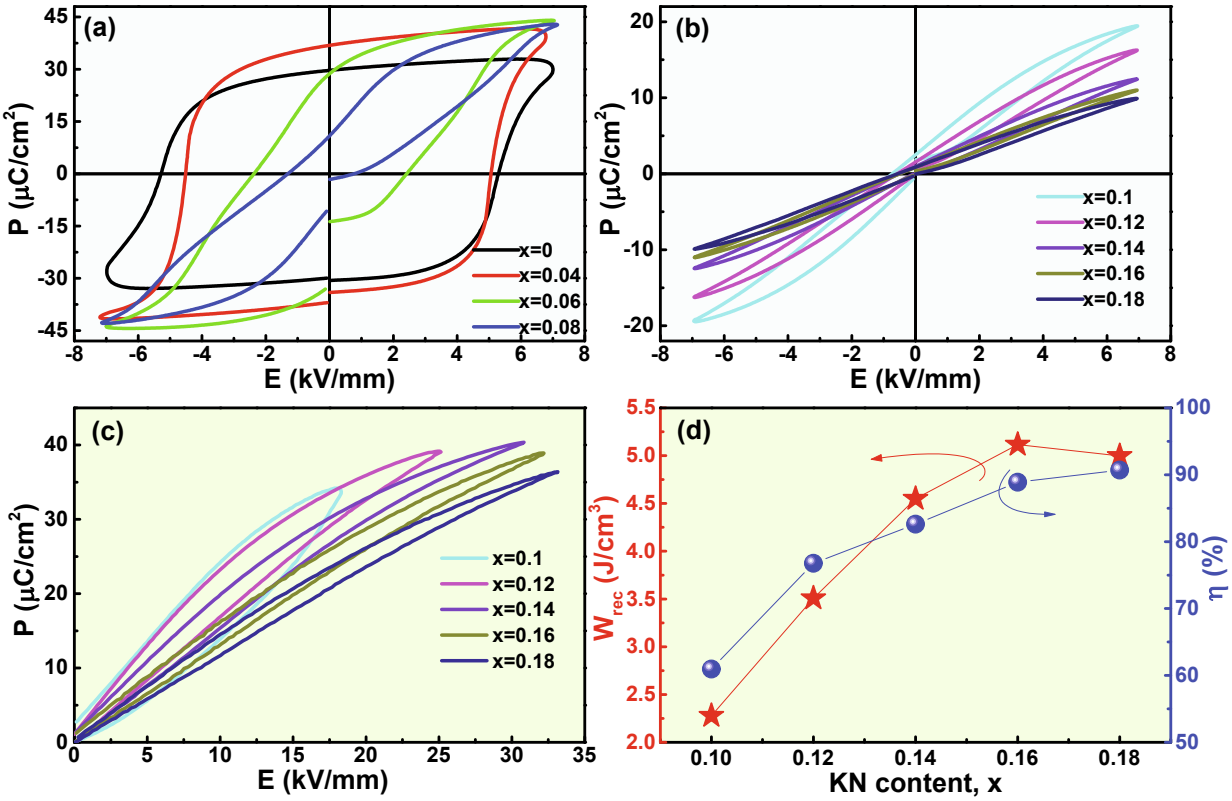

Fig. 3. *P-E* loops of (1-*x*)BNT-*x*KN ceramics under (a, b) 7 kV/mm and (c) maximum testable electric fields at a fixed frequency of 10 Hz; (d) the evolution of W_{rec} and η values with changing KN content.

Before the SEM observation, the samples were polished and thermally etched at 1000 °C for 30 min. The density of the as-sintered ceramics was achieved by the Archimedes method. The dielectric breakdown measurement was performed at room temperature by using a voltage-withstand test device (BDJC-50KV, Beiguangjingyi Instrument Equipment Co. Ltd., Beijing, China). The temperature and frequency dependent *P-E* loops were measured using a ferroelectric test system (Precision multiferroelectric; Radiant Technologies Inc, Albuquerque, New Mexico) connected to a high-temperature probing stage (HFS600E-PB2, Linkam Scientific Instruments, Tadworth, UK). The energy release properties of the ceramic disk capacitor were investigated by a commercial charge-discharge platform (CFD-001, Gogo Instruments Technology, Shanghai, China). For the dielectric breakdown, the *P-E* loops and the pulsed charge-discharge test, the sample size is about 0.15 mm (thickness) × 7 mm^2 (electrode area).

3. Results and discussion

Fig. 1(a) presents room-temperature XRD results of (1-*x*)BNT-*x*KN ceramics. A typical perovskite structure can be identified for all studied samples. By looking into the diffraction peak approximately at $2\theta \sim 39°$ and 47° in Fig. 1(b) and (c), respectively, a doublet *(1 1 1)* peak and a singlet *(2 0 0)* peak as well as an obvious *(3 1 1)/2* superlattice diffraction peak can be seen for samples with *x* up to 0.06, typical of rhombohedral *R3c* symmetry. The split *(1 1 1)* diffraction lines gradually emerge together with increasing KN content, and at the same time the intensity of *(3 1 1)/2* superlattice diffraction peak decreases monotonously. A singlet *(1 1 1)* peak and a singlet *(2 0 0)* peak can be observed in the absence of *(3 1 1)/2* peak in the compositions of $x \geq 0.08$, indicating a pseudocubic average structure. The room temperature Raman spectra and the wavenumber of Raman peaks achieved from deconvolution results by Gauss-Lorentz shape functions are shown in Fig. 1(d) and (e). From the local structure point of view, the *ν4* Raman mode, which corresponds to the double-degenerate O-B-O stretching vibration with oxygen situated along the *c*-axis [34], can be found in the compositions with $x > 0.06$, indicating that the local structure symmetry of these compositions should be tetragonal. The inconsistency between average and local structures should be related to the disruption of long-range FE or AFE ordering, as reflected by enhanced dielectric relaxation behavior, as shown in Fig. 1(f). The pure BNT was known to exhibit a nonergodic relaxor FE state at room temperature, which can be confirmed by an electric field induced dielectric anomaly corresponding to the FE-relaxor phase transition at $T_{FR}^{'}$ during heating for poled samples. Moreover, another dielectric anomaly related to the transition between *R3c* FE and *P4bm* AFE phases can be seen at $T_{R\text{-}T} \sim 320$ °C. With increasing KN content, both $T_{FR}^{'}$ and $T_{R\text{-}T}$ decrease monotonously, leading to the room-temperature phase transition from nonergodic relaxor rhombohedral FE phase to ergodic relaxor FE phase at x = 0.06, and then to relaxor AFE tetragonal phase at $x = 0.08$, as can be clearly shown in Fig. 1(g). Accompanying the evolution of local structure and dielectric relaxation behavior, an adjustable room-temperature dielectric permittivity can be observed, ranging from ~850 to 2100. The formation of relaxor characteristics clearly enhances the dielectric response of (1-*x*)BNT-*x*KN solid solutions with larger *x*.

Fig. 2(a)–(d) show the grain morphology of (1-*x*)BNT-*x*KN ceramics sintered at their optimum temperatures. Dense microstructure with high density ~97% and ultrafine grains can be observed for all the studied samples. According to the fitting results of the grain size distribution shown in the inset of the corresponding SEM image, the average grain size (G_a) gradually decreases from ~0.68 μm at $x = 0$ to ~0.47 μm at $x = 0.18$. The formation of submicron grains should be attributed to the formation of low-viscosity glass phase of SiO_2-K_2O during sintering, which effectively promotes the densification at a relatively low temperature, but simultaneously suppresses the grain growth by warping up the particles. The achievement of fine grains

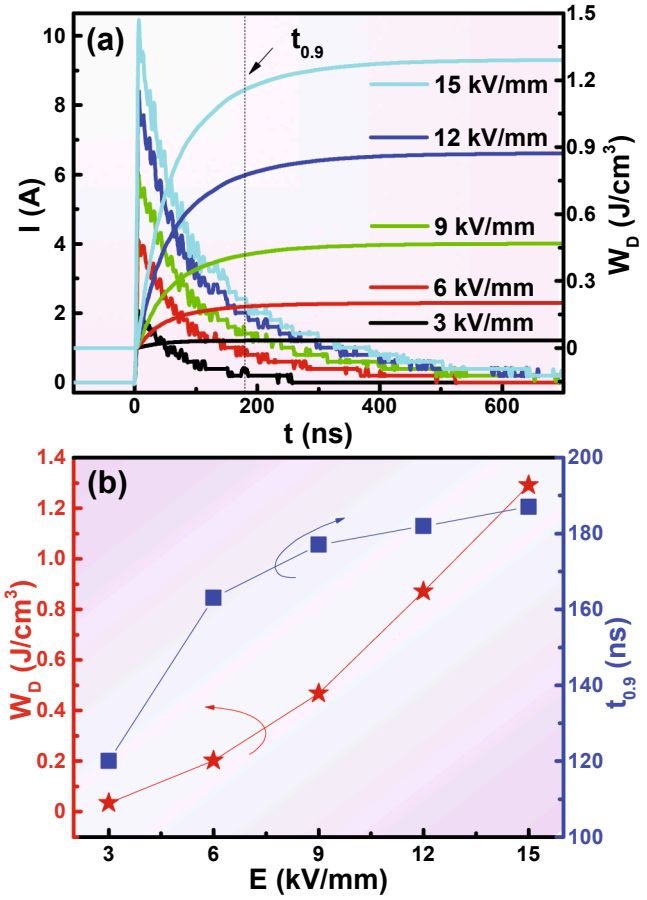

Fig. 4. (a) Room-temperature pulsed overdamped discharging current (*I-t*) curves and discharge energy density (W_D-*t*) curves for the $x = 0.16$ ceramic at a fixed load resistance of 200 Ω under various electric fields, and (b) the variation of overall W_D and $t_{0.9}$ as a function of applied electric field.

should also be in favor of the dielectric breakdown behavior as a result of the high resistivity of grain boundaries. The E_B values have an exponential decay relationship with grain size, i.e., $E_B \propto (G_a)^{-a}$, with exponent values in the range of 0.2–0.4 [5,35]. The improved E_B value with decreasing grain size can be directly confirmed by using the *Weibull* distribution measurement [5,36], as shown in Fig. 2(e) and (f). All detected data points fit well with a linear relation with a *Weibull* modulus *m* more than five, demonstrating high reliability of the *Weibull* analysis. The average E_B was found to increase monotonously with increasing KN content in the studied composition range, on the order of 18 and 36 kV/mm for $x = 0$ and $x = 0.18$ ceramics, respectively.

The *P-E* loops of (1-*x*)BNT-*x*KN ceramics measured under 7 kV/mm are displayed in Fig. 3(a) and (b). Typical nonergodic relaxor FE with a square *P-E* loop at $x = 0$ gradually evolves into the coexisting state of nonergodic and ergodic FEs with a pinched *P-E* loop at $x = 0.06$–0.08. However, linear-like polarization response at $x > 0.1$ should stem from the *P4bm* AFE phase because obviously enhanced dielectric relaxation behavior provides an obstacle for the field induced AFE to FE phase transition by introducing large random electric field. For the evaluation of energy-storage properties, unipolar *P-E* loops for compositions of $x \geq 0.1$ under their corresponding maximum testable electric fields are given in Fig. 3(c). Near-zero P_r values can be detected for all studied samples, indicating completely reversible field-induced AFE to FE phase transition. Furthermore, obviously increased testable electric field and decreased polarization hysteresis can be seen with increasing KN content, leading to slimmer and slimmer *P-E* loops. The calculated W_{rec} and η values with changing x are summarized in Fig. 3(d). With the substitution of KN, the η value increases monotonously, while the W_{rec} value increases firstly and then reaches its maximum value at $x = 0.16$ and finally decreases with further increasing x. Excellent comprehensive energy storage performances with simultaneously high $W_{rec} \sim 5.2$ J/cm^3 and $\eta \sim 88\%$ were achieved at $x = 0.16$ under an electric field of 32 kV/mm.

To evaluate actual energy charge and release performances of practical capacitor applications, the over-damped pulsed discharge electric current-time (*I-t*) curves and the discharge energy density vs. time curves ($W_D = R\int I(t)^2 dt/V$, *R* is the load resistor of 200 Ω and *V* is the sample volume) under different electric fields are shown in Fig. 4(a). The overall W_D value monotonously increases from 0.05 J/cm^3 to 1.29 J/cm^3 as electric field increases from 3 kV/mm to 15 kV/mm, as shown in Fig. 4(b). Moreover, 90% stored energy can be released within a short time $t_{0.9} < 200$ ns under the studied electric fields as a result of the fast polarization response of APNRs to external electric fields.

In order to evaluate the stability of the energy storage properties, *P-E* loops at different temperatures and frequencies as well as the corresponding calculated W_{rec} and η values for the $x = 0.16$ ceramic are revealed in Fig. 5. Owing to the strong random field, linear-like polarization response can be obtained under 20 kV/mm. With increasing temperature, the decrease in size of APNRs would lead to an increase in the rate of their response to external electric field as a result of enhanced dynamics. As a result, linear-like *P-E* loops can be achieved in the studied temperature range, leading to the achievement of higher η than 90%. At the same time, based on thermally stable dielectric response on heating (see Fig. 1(f)), temperature insensitive W_{rec} (2.1–2.4 J/cm^3) can be obtained in the temperature range of 25–200 °C. P_{max} slightly decreases from 26.3 μC/cm^2 to 25.7 μC/cm^2 as measuring frequency increases from 0.1 Hz to 100 Hz. Therefore, a large W_{rec} of 2.27–2.37 J/cm^3 and a high η of 89.0%-92.8% can be found in the studied frequency range from 0.1 Hz to 100 Hz. The achievement of linear-like *P-E* loops in the whole measuring temperature and frequency range demonstrates an excellent stability of energy-storage properties against the measurement conditions.

A comparison of W_{rec}, η and corresponding applied electric field magnitudes between the $x = 0.16$ ceramic and some representative lead-free ceramics is shown in Fig. 6(a)–(c) [4–6,7–25]. For most of relaxor FE ceramics, relatively high η values usually accompany relatively low W_{rec} values. This is generally ascribed to the fast polarization saturation under a low electric field for most relaxor FEs. In addition, (Na,K)NbO_3 (NKN), $BaTiO_3$ (BT) and $SrTiO_3$ (ST)-based relaxor FEs exhibit low spontaneous polarizations, while $BiFeO_3$ (BF) and $(Bi_{0.5}K_{0.5})TiO_3$-based compositions usually have large loss and relatively low E_B. By comparison, $NaNbO_3$ (NN) and $AgNbO_3$ (AN)-based normal AFE ceramics can be found to exhibit advantages in achieving large W_{rec} values (see Fig. 6(a) and (b)), yet over 25% of the stored energy during charging cannot be utilized but transforms into heat, also leading to increased possibility of the thermal breakdown. The introduction of relaxor characteristics into AFEs leads to the improvement of η values on the basic of high W_{rec}. As a result, a good balance between both large W_{rec} and high η was realized in the studied ceramic. Moreover, it can be seen that the W_{rec} value of the $x = 0.16$ ceramic is superior to that of most lead-free bulk ceramics. There should be some reasons behind in compositional design or polarization-field response of the $x = 0.16$ ceramic. Fig. 6(c) shows W_{rec} values against applied electric field magnitudes for various lead-free ceramics, in which the dotted parabolic curves indicate the theoretical energy-storage density calculated from $W_{cal} = \varepsilon_r \varepsilon_0 E^2/2$ for linear dielectrics with different dielectric permittivity. It can be empirically concluded that the ceramic with medium ε_r on the order of one thousand can bring its superiority into full play in energy-storage properties. Although the $x = 0.16$ sample is located at the dotted parabolic curve with $\varepsilon_r \sim 1200$, it has a slightly higher ε_r of ~1500 as a result of the nonlinear dielectric response under high fields for relaxor AFEs/FEs. This can be clearly seen from Fig. 6(d) where the real *P-E* loop of the $x = 0.16$ sample was

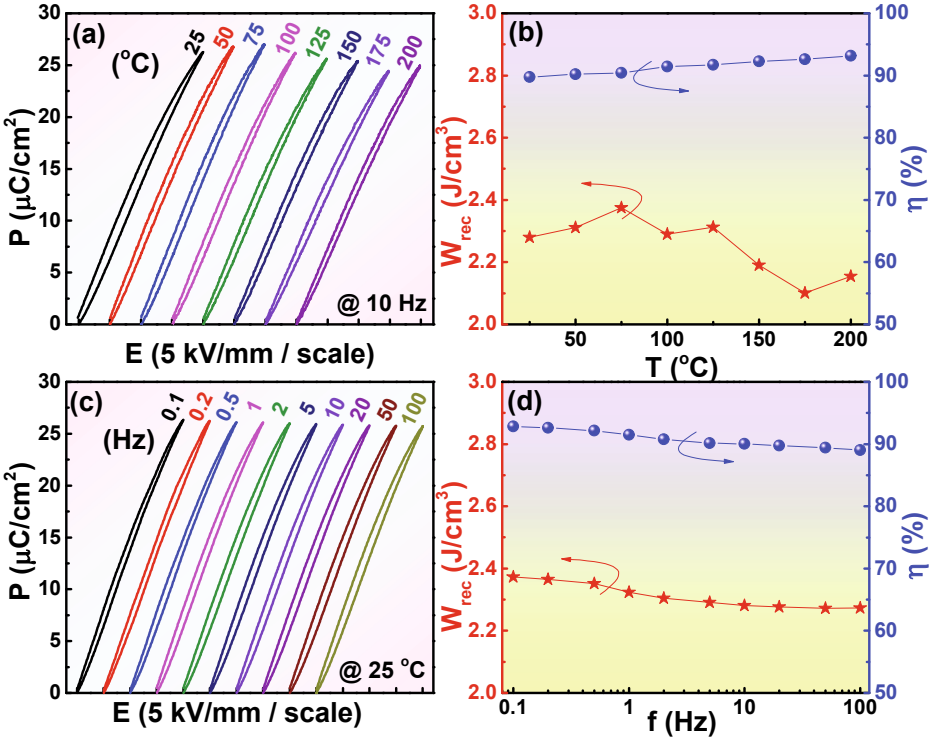

Fig. 5. (a) *P-E* loops, (b) W_{rec} and η values as a function of measuring temperature, (c) *P-E* loops and (d) W_{rec} and η values at room temperature as a function of measuring frequency for the $x = 0.16$ ceramic.

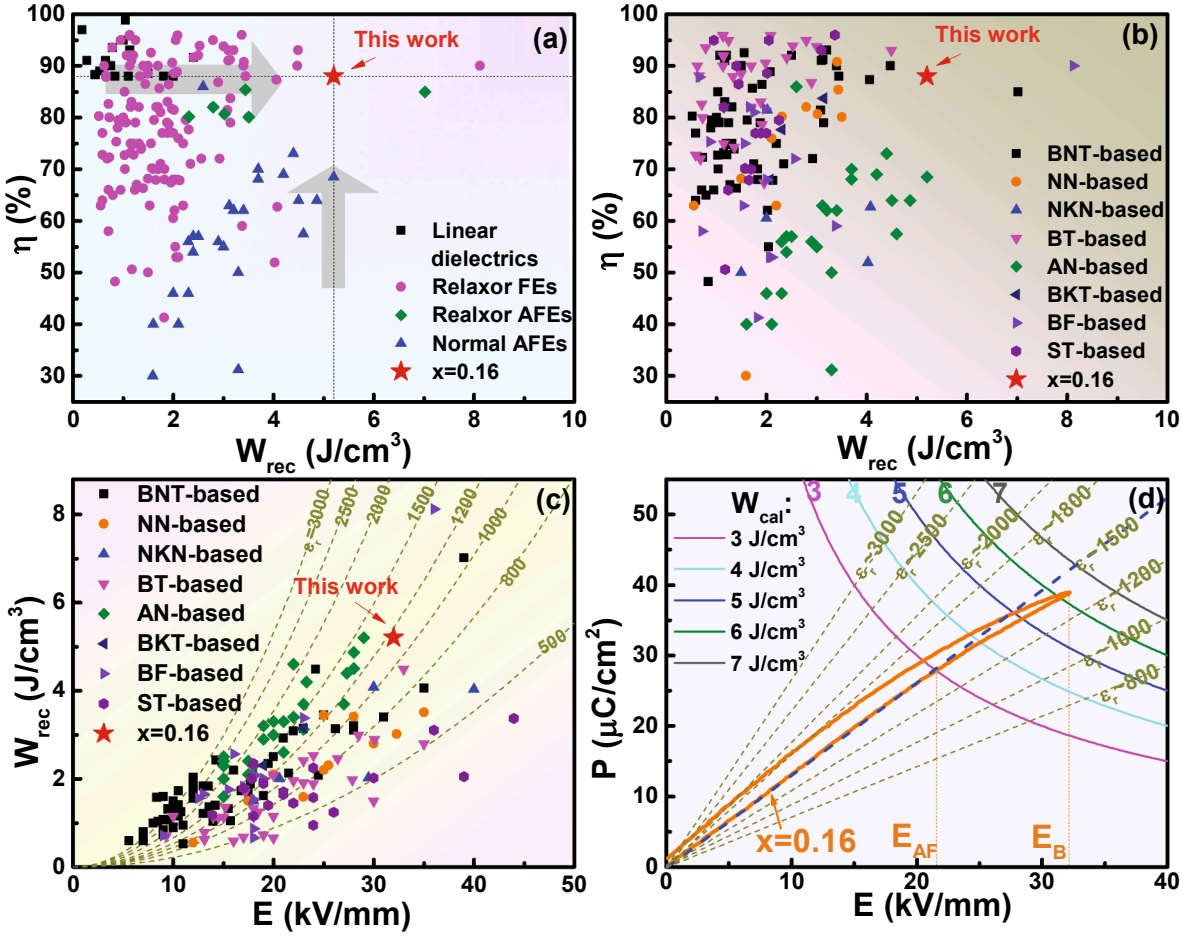

Fig. 6. A comparison of (a, b) W_{rec} and η, and (c) W_{rec} and applied electric field magnitude between the $x = 0.16$ ceramic and some other bulk lead-free ceramics; (d) the measured *P-E* loop for the $x = 0.16$ ceramic and the theoretical *P-E* relation for linear dielectrics with different ε_r and W_{rec}.

plotted together with theoretical *P-E* relations ($W_{rec} = P{\cdot}E/2$ and $\varepsilon_r{\cdot}\varepsilon_o = P/E$) of linear dielectrics. The curved polarization response of the $x = 0.16$ sample can be simply divided into a linear part under low fields and a nonlinear part under high fields (above E_{AF}). The formation of relaxor characteristics in the studied compositions greatly helps delay the AFE-FE phase transition through increasing E_{AF}, leading to expansion of the linear polarization-response part and shrinkage of the nonlinear response part. This enables us better understand why the $x = 0.16$ ceramic shows large advantages in comprehensive energy-storage owing to both appropriate ε_r and desired polarization response feature.

4. Conclusions

(1-*x*)BNT-*x*KN lead-free solid solution ceramics have been prepared via a traditional solid-state reaction method. Addition of a small amount of KN was found to induce an obvious phase structure transition, and simultaneously stabilize high-temperature relaxor AFE *P4bm* phase close to room temperature, leading to an adjustable room-temperature permittivity between 850 and 2100. As a result, excellent comprehensive energy-storage performances of W_{rec} of ~5.2 J/cm^3, large η of ~88%, fast discharge rate of $t_{0.9} < 200$ ns and outstanding temperature and frequency stability ($W_{rec} \sim$ 2.1–2.4 J/cm^3 and $\eta > 89\%$ under 20 kV/mm in the range of 25–200 °C and 0.1–100 Hz) at $x = 0.16$ owing to thermally-stable and medium dielectric response, linear-like polarization response and enhanced E_B values. The results provide a useful guidance for designing advantageous energy-storage dielectric compositions, and demonstrate that BNT-KN lead-free relaxor AFEs have outstanding potentials in future pulse power applications.

Declaration of Competing Interest

There are no conflicts to declare.

Acknowledgements

This work was financially supported by National Natural Science Foundation of China (Grant No. U19A2087 and U1432113).

References

[1] B.J. Chu, X. Zhou, K.L. Ren, B. Neese, M.R. Lin, Q. Wang, F. Bauer, Q.M. Zhang, A dielectric polymer with high electric energy density and fast discharge speed, Science 313 (2006) 334–336.
[2] H. Pan, F. Li, Y. Liu, Q.H. Zhang, M. Wang, S. Lan, Y.P. Zheng, J. Ma, L. Gu, Y. Shen, P. Yu, S.J. Zhang, L.-Q. Chen, Y.-H. Lin, C.-W. Nan, Ultrahigh-energy density lead-free dielectric films via polymorphic nanodomain design, Science 365 (2019) 578–582.
[3] H. Qi, R.Z. Zuo, A.W. Xie, A. Tian, J. Fu, Y. Zhang, S.J. Zhang, Ultrahigh energy-storage density in $NaNbO_3$-based lead-free relaxor antiferroelectric ceramics with nanoscale domains, Adv. Funct. Mater. (2019) 1903877.
[4] G. Wang, J.L. Li, X. Zhang, Z.M. Fan, F. Yang, A. Feteira, D. Zhou, D.C. Sinclair, T. Ma, X.L. Tan, D.W. Wang, I.M. Reaney, Ultrahigh energy storage density lead-free multilayers by controlled electrical homogeneity, Energy Environ. Sci. 12 (2019) 582–588.
[5] L.T. Yang, X. Kong, F. Li, H. Hao, Z.X. Cheng, H.X. Liu, J.F. Li, S.J. Zhang, Perovskite lead-free dielectrics for energy storage applications, Prog. Mater. Sci. 102 (2019) 72–108.
[6] A. Chauhan, S. Patel, R. Vaish, C.R. Bowen, Anti-ferroelectric ceramics for high energy density capacitors, Materials 8 (2015) 8009–8031.
[7] J.Y. Wu, A. Mahajan, L. Riekehr, H.F. Zhang, B. Yang, N. Meng, Z. Zhang, H.X. Yan, Perovskite $Sr_x(Bi_{1-x}Na_{0.97-x}Li_{0.03})_{0.5}TiO_3$ ceramics with polar nano regions for high power energy storage, Nano Energy 50 (2018) 723–732.
[8] H. Qi, A.W. Xie, A. Tian, R.Z. Zuo, Superior energy-storage capacitors with simultaneously giant energy density and efficiency using nanodomain engineered $BiFeO_3$-$BaTiO_3$-$NaNbO_3$ lead-free bulk ferroelectrics, Adv. Energy Mater. (2019) 201903338.
[9] N.T. Liu, R.H. Liang, Z.Y. Zhou, X.L. Dong, Designing lead-free bismuth ferrite-based ceramics learning from relaxor ferroelectric behavior for simultaneous high energy density and efficiency under low electric field, J. Mater. Chem. C 6 (2018) 10211–10217.
[10] T.Q. Shao, H.L. Du, H. Ma, S.B. Qu, J. Wang, J.F. Wang, X.Y. Wei, Z. Xu, Potassium-sodium niobate based lead-free ceramics: novel electrical energy storage materials, J. Mater. Chem. A 5 (2017) 554–563.
[11] Q.B. Yuan, G. Li, F.Z. Yao, S.D. Cheng, Y.F. Wang, R. Ma, S.B. Mi, M. Gu, K. Wang, J.F. Li, H. Wang, Simultaneously achieved temperature-insensitive high energy density and efficiency in domain engineered $BaTiO_3$-$Bi(Mg_{0.5}Zr_{0.5})O_3$ lead-free relaxor ferroelectrics, Nano Energy 52 (2018) 203–210.
[12] M.X. Zhou, R.H. Liang, Z.Y. Zhou, X.L. Dong, Novel $BaTiO_3$-based lead-free ceramic capacitors featuring high energy storage density, high power density, and excellent stability, J. Mater. Chem. C 6 (2018) 8528–8537.
[13] H. Qi, R.Z. Zuo, Linear-like lead-free relaxor antiferroelectric $(Bi_{0.5}Na_{0.5})TiO_3$-$NaNbO_3$ with giant energy-storage density/efficiency and super stability against temperature and frequency, J. Mater. Chem. A 7 (2019) 3971–3978.
[14] C.Q. Zhu, Z. Cai, B.C. Luo, L.M. Guo, L.T. Li, X.H. Wang, High temperature lead-free BNT-based ceramics with stable energy storage and dielectric properties, J. Mater. Chem. A 8 (2020) 683–692.
[15] X.S. Qiao, F.D. Zhang, D. Wu, B. Chen, X.M. Zhao, Z.H. Peng, X.D. Ren, P.F. Liang, X.L. Chao, Z.P. Yang, Superior comprehensive energy storage properties in $Bi_{0.5}Na_{0.5}TiO_3$-based relaxor ferroelectric ceramics, Chem. Eng. J. 388 (2020) 124158.
[16] D. Hu, Z.B. Pan, X. Zhang, H.R. Ye, Z.Y. He, M.K. Wang, S. Xing, J.W. Zhai, Q. Fu, J.J. Liu, Greatly enhanced discharge energy density and efficiency of novel relaxation ferroelectric BNT-BKT-based ceramics, J. Mater. Chem. C 8 (2020) 591–601.
[17] D. Li, Y. Lin, M. Zhang, H.B. Yang, Achieved ultrahigh energy storage properties and outstanding charge-discharge performances in $(Na_{0.5}Bi_{0.5})_{0.7}Sr_{0.3}TiO_3$-based ceramics by introducing a linear additive, Chem. Eng. J. 392 (2020) 123729.
[18] Y. Lin, D. Li, M. Zhang, H.B. Yang, $(Na_{0.5}Bi_{0.5})_{0.7}Sr_{0.3}TiO_3$ modified by $Bi(Mg_{2/3}Nb_{1/3})O_3$ ceramics with high energy-storage properties and an ultrafast discharge rate, J. Mater. Chem. C 8 (2020) 2258–2264.
[19] F. Li, X. Hou, T.Y. Li, R.J. Si, C.C. Wang, J.W. Zhai, Fine-grain induced outstanding energy storage performance in novel $Bi_{0.5}K_{0.5}TiO_3$-$Ba(Mg_{1/3}Nb_{2/3})O_3$ ceramics via hot-press strategy, J. Mater. Chem. C 7 (2019) 12127–12138.
[20] W. Wang, Y.P. Pu, X. Guo, R.K. Shi, Y. Shi, M.D. Yang, J.W. Li, X. Peng, Y. Li, Enhanced energy storage density and high efficiency of lead-free $Ca_{1-x}Sr_xTi_{1-y}Zr_yO_3$ linear dielectric ceramics, J. Eur. Ceram. Soc. 39 (2019) 5236–5242.
[21] Z.T. Yang, H.L. Du, L. Jin, Q.Y. Hu, H. Wang, Y.F. Li, J.F. Wang, F. Gao, S.B. Qu, Realizing high comprehensive energy storage performance in lead-free bulk ceramics via designing an unmatched temperature range, J. Mater. Chem. A 7 (2019) 27256–27266.
[22] Y. Tian, L. Jin, H.F. Zhang, Z. Xu, X.Y. Wei, E.D. Politova, S.Y. Stefanovich, N.V. Tarakina, I. Abrahams, H.X. Yan, High energy density in silver niobate ceramics, J. Mater. Chem. A 4 (2016) 17279–17287.
[23] L. Zhao, Q. Liu, J. Gao, S.J. Zhang, J.F. Li, Lead-free antiferroelectric silver niobate tantalate with high energy storage performance, Adv. Mater. 29 (2017) 1701824.
[24] N.N. Luo, K. Han, F.P. Zhuo, C. Xu, G.Z. Zhang, L.J. Liu, X.Y. Chen, C.Z. Hu, H.F. Zhou, Y.Z. Wei, Aliovalent A-site engineered $AgNbO_3$ lead-free antiferroelectric ceramics toward superior energy storage density, J. Mater. Chem. A 7 (2019) 14118–14128.
[25] X.H. Liu, Y. Li, X.H. Hao, Ultra-high energy-storage density and fast discharge speed of $(Pb_{0.98-x}La_{0.02}Sr_x)(Zr_{0.9}Sn_{0.1})_{0.995}O_3$ antiferroelectric ceramics prepared via the tape-casting method, J. Mater. Chem. A 7 (2019) 11858–11866.
[26] D.S. Fu, H. Taniguchi, M. Itoh, S. Koshihara, N. Yamamoto, S. Mori, Relaxor Pb $(Mg_{1/3}Nb_{2/3})O_3$: a ferroelectric with multiple inhomogeneities, Phys. Rev. Lett. 103 (2009) 207601.
[27] H.R. Jo, C.S. Lynch, A high energy density relaxor antiferroelectric pulsed capacitor dielectric, J. Appl. Phys. 119 (2016) 024104.
[28] P. Mohapatra, Z.M. Fan, J. Cui, X.L. Tan, Relaxor antiferroelectric ceramics with ultrahigh efficiency for energy storage applications, J. Eur. Ceram. Soc. 39 (2019) 4735–4742.
[29] H. Qi, R.Z. Zuo, Giant electrostrictive strain in $(Bi_{0.5}Na_{0.5})TiO_3$-$NaNbO_3$ lead-free relaxor antiferroelectrics featuring temperature and frequency stability, J. Mater. Chem. A 8 (2020) 2369–2375.
[30] D. Schütz, M. Deluca, W. Krauss, A. Feteira, T. Jackson, K. Reichmann, Lone-pair-induced covalency as the cause of temperature and field-induced instabilities in bismuth sodium titanate, Adv. Funct. Mater. 22 (2012) 2285–2294.
[31] G.O. Jones, P.A. Thomas, Investigation of the structure and phase transitions in the novel A-site substituted distorted perovskite compound $Na_{0.5}Bi_{0.5}TiO_3$, Acta Cryst. B 58 (2002) 168–178.
[32] G. Wang, Y.Z. Li, C.A. Murray, C.C. Tang, D.A. Hall, Thermally-induced phase transformations in $Na_{0.5}Bi_{0.5}TiO_3$-$KNbO_3$ ceramics, J. Am. Ceram. Soc. 100 (2017) 3293–3304.
[33] Y. Hiruma, H. Nagata, T. Takenaka, Phase diagrams and electrical properties of $(Bi_{1/2}Na_{1/2})TiO_3$-based solid solutions, J. Appl. Phys. 104 (2008) 124106.
[34] K. Kakimoto, K. Akao, Y.P. Guo, H. Ohsato, Raman scattering study of piezoelectric $(Na_{0.5}K_{0.5})NbO_3$-$LiNbO_3$ ceramics, Jpn. J. Appl. Phys. 44 (2005) 7064–7067.
[35] T. Tunkasiri, G. Rujijanagul, Dielectric strength of fine grained barium titanate ceramics, J. Mater. Sci. Lett. 15 (1996) 1767–1769.
[36] W. Weibull, A statistical distribution function of wide applicability, J. Appl. Mech. 18 (1951) 293–297.